ORNL/SPR-2025/4019
M3LW-25OR0403023

Light Water Reactor Sustainability Program

Developing Ultrasonic Nondestructive Sensing Techniques for Rebar Stress Measurement Using the Acoustoelastic Effect

Hongbin Sun
Samantha Sabatino
Adam Brooks
Marco Martinez
Mohammed Alnaggar

August 2025

U.S. Department of Energy
Office of Nuclear Energy

ORNL/SPR-2025/4019
M3LW-25OR0403023

Developing Ultrasonic Nondestructive Sensing Techniques for Rebar Stress Measurement Using the Acoustoelastic Effect

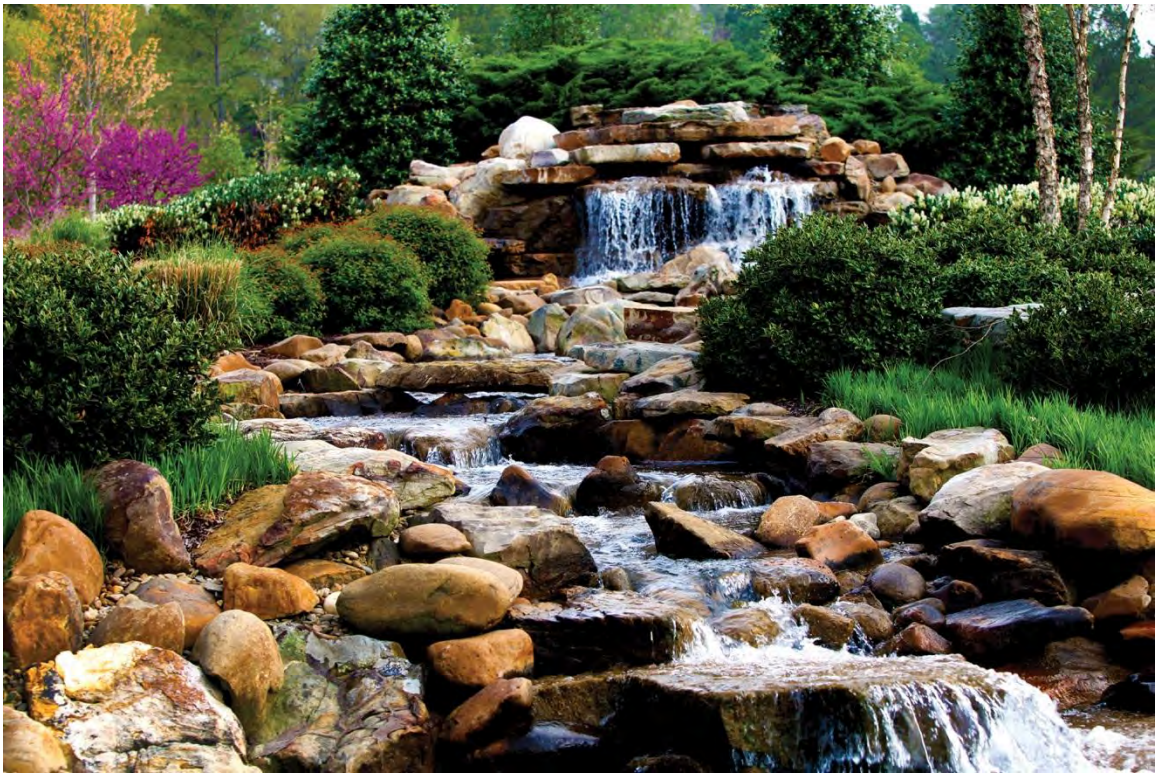

Hongbin Sun
Samantha Sabatino
Adam Brooks
Marco Martinez
Mohammed Alnaggar

August 2025

OAK RIDGE National Laboratory

ORNL IS MANAGED BY UT-BATTELLE LLC FOR THE US DEPARTMENT OF ENERGY

ORNL/SPR-2025/4019
M3LW-25OR0403023

Light Water Reactor Sustainability Program

M3LW-25OR0403023

Nuclear Energy and Fuel Cycle Division

DEVELOPING ULTRASONIC NONDESTRUCTIVE SENSING TECHNIQUES FOR REBAR STRESS MEASUREMENT USING THE ACOUSTOELASTIC EFFECT

Hongbin Sun
Samantha Sabatino
Adam Brooks
Marco Martinez
Mohammed Alnaggar

August 2025

Prepared by
OAK RIDGE NATIONAL LABORATORY
Oak Ridge, TN 37831
managed by
UT-BATTELLE LLC
for the
US DEPARTMENT OF ENERGY
under contract DE-AC05-00OR22725

CONTENTS

LIST OF FIGURES

LIST OF TABLES

EXECUTIVE SUMMARY

This report presents a comprehensive evaluation of ultrasonic non-destructive evaluation (NDE) techniques for quantifying tensile stress in steel rebar, with the specific application to reinforced concrete structures in nuclear facilities. The focus is on ultrasonic methods that utilize the acoustoelastic effect, in which ultrasonic wave velocity varies with internal stress. The objective of this work is to develop field-deployable diagnostics capable of assessing embedded rebar stress without requiring destructive sampling.

Residual and applied stresses in steel reinforcement significantly influence the structural integrity and longevity of reinforced concrete. Existing in situ measurement methods, such as strain gauges or core removal, are often impractical for shielded or operational infrastructure. Ultrasonic NDE offers advantages in portability, sensitivity to subsurface stress states, and minimal surface preparation, making it a promising alternative for embedded rebar assessment.

An experimental program was conducted to establish the quantitative relationship between tensile stress and ultrasonic wave velocity in steel rebar. The study employed #6 and #8 Grade 60 rebars subjected to controlled tensile loading and unloading cycles. A customized ultrasonic monitoring system was implemented using 5 MHz contact transducers and a pulser–receiver system. High-resolution signal acquisition was achieved through waveform averaging and synchronized recording of load, strain, temperature, and ultrasonic signals. Coda wave interferometry and a stretching algorithm were used to detect small velocity changes associated with applied stress.

The results demonstrate a strong, consistent linear correlation between ultrasonic velocity and tensile stress across all tests, except for one initial low-stress run. The velocity–stress sensitivity remained within a narrow range despite variations in loading rate and peak stress levels. This result confirmed the robustness and repeatability of the acoustoelastic response. Consistent with the thermoelastic effect, thermal measurements revealed a characteristic decrease in temperature during elastic loading and an increase during unloading. This behavior validates the physical basis of the ultrasonic measurements and highlights the importance of incorporating temperature compensation in future field implementations. Multiple load–unload cycles confirmed the repeatability of the stress–velocity relationship. The consistency of linear regression slopes during both loading and unloading phases further supports the feasibility of applying this technique for real-time monitoring. Minor deviations were attributed to initial residual manufacturing stress or environmental temperature fluctuations.

The findings confirm that ultrasonic acoustoelastic methods are technically viable for internal stress evaluation in rebar. The study provides empirical support for extending this technique to in situ applications in civil and nuclear infrastructure. The results suggest that ultrasonic NDE can be deployed as a non-invasive, accurate diagnostic tool for monitoring structural integrity. Future efforts should focus on developing automated temperature compensation strategies, enhancing sensor attachment methods to prevent signal loss during high loads, and integrating the system into embedded sensor platforms for continuous field monitoring. This work represents a critical step toward implementing ultrasonic stress measurement technology in mission-critical structures where safety, reliability, and non-invasiveness are paramount.

ABBREVIATIONS

J-PARC	the Japan Proton Accelerator Research Complex
LCR	longitudinal critically refracted
NDE	non-destructive evaluation
SMFL	spontaneous magnetic flux leakage
TAKUMI	the Engineering Materials Diffractometer
TOF	time-of-flight

ACKNOWLEDGMENTS

This research was sponsored by the US Department of Energy Office of Nuclear Energy's Light Water Reactor Sustainability (LWRS) Program under contract DE-AC05-00OR22725 with UT Battelle LLC/Oak Ridge National Laboratory. Work was done under the Materials Research Pathway as part of the Concrete NDE of Civil Structures Task. Shane Hawkins and Mechanical Properties and Mechanics Servo-Hydraulic Testing Facility are acknowledged for their support on the rebar tensile testing. Xiang (Frank) Chen is acknowledged for his invaluable efforts in project management. Paula Bran Anleu is also acknowledged for her comments on the early draft of this report.

1. INTRODUCTION

The accurate characterization of residual and applied stresses within structural components is essential for ensuring the safety, reliability, and longevity of engineered systems. Residual stresses, which develop during manufacturing, processing, or service loading, can significantly influence fatigue performance, crack initiation, and failure modes in structural materials. In reinforced concrete systems, which are ubiquitous in civil infrastructure and nuclear facilities, embedded steel rebar serves as the primary load-carrying element under tension. The long-term performance of these systems depends heavily on the internal stress states of the reinforcement, and these states are not directly observable once encased in concrete. Developing reliable, non-destructive techniques to assess these stresses is therefore critically important, especially in the context of aging infrastructure, seismic risk zones, and high-radiation environments such as nuclear power plants.

Conventional stress measurement techniques such as strain gauges, extensometers, or destructive sampling offer only localized, surface-level, or intrusive evaluations. These methods are often impractical or infeasible in field scenarios, especially in heavily shielded or in-service structures where direct access to the rebar is not possible. As the nuclear power sector begins to prioritize life-extension, and long-term stewardship of critical infrastructure, the need for accurate, non-invasive diagnostic tools is even more urgent.

This report addresses this gap by exploring and validating ultrasonic-based non-destructive evaluation (NDE) techniques, particularly those leveraging the acoustoelastic effect, for internal stress monitoring in steel reinforcement. Ultrasonic methods offer several advantages: they are relatively low-cost, portable, sensitive to subsurface conditions, and adaptable to field deployment. These characteristics make ultrasonic methods ideal candidates for evaluating embedded steel in reinforced concrete without requiring core removal or sample destruction.

To provide a foundation for this work, a comprehensive literature review is presented that summarizes three major NDE methodologies commonly explored for residual stress quantification: (1) ultrasonic techniques based on the acoustoelastic effect, (2) diffraction-based methods such as neutron and X-ray diffraction, and (3) magnetic methods tailored to ferromagnetic materials like steel. While diffraction methods offer exceptional accuracy and depth resolution, they require access to large, specialized facilities and are not deployable in the field. Similarly, magnetic techniques show theoretical promise but suffer from limitations related to surface accessibility, calibration complexity, and measurement reliability when the rebar is embedded in concrete. Ultrasonic methods, by contrast, represent a balance between sensitivity, portability, and field feasibility, particularly when advanced signal processing techniques are employed.

The primary motivation behind the experimental program described herein is to establish a quantitative, real-time relationship between applied rebar stress and ultrasonic wave velocity in steel rebar under controlled loading conditions. This relationship is governed by the acoustoelastic effect, which predicts that ultrasonic wave speeds vary in proportion to the internal stress state of the material. However, capturing this effect in practical settings is challenging due to small signal variations, environmental noise, and temperature fluctuations.

To address these challenges, the research team designed and implemented a robust experimental setup to simultaneously measure mechanical load, temperature, and ultrasonic signal response during tensile loading of steel rebar specimens. A series of tensile tests were conducted on #8 rebar samples (1 in. in diameter, 16 in. long) under incremental load–unload cycles. Ultrasonic transducers were mounted on the surface of the rebar using a fixed epoxy-based coupling method. A thermocouple was installed at the

midpoint to monitor temperature variations throughout the test, which are known to influence ultrasonic velocity through the thermoelastic effect. A 5 MHz ultrasonic transducer system integrated with a pulser–receiver and digital oscilloscope was used to transmit and receive ultrasonic signals. A high signal-to-noise ratio was achieved through waveform averaging, and data were recorded at five-second intervals.

Advanced signal processing algorithms with coda wave interferometry were used to detect relative changes in wave velocity. This method allows for the quantification of very small stress-induced velocity shifts by correlating perturbed waveforms with a baseline reference signal. Emphasis was placed on analyzing coda waves—scattered components of the ultrasonic signal that are particularly sensitive to microstructural changes and stress fields within the bulk of the material.

Experimental results confirm a strong and repeatable linear correlation between ultrasonic velocity and applied stress for both loading and unloading phases. Thermoelastic coupling effects were also observed, as evidenced by reversible temperature shifts and associated velocity changes. These findings provide strong empirical support for the use of ultrasonic NDE methods for embedded stress monitoring. An important finding is that the variation in slope between loading and unloading cycles suggests that additional phenomena, such as residual stress redistribution or microplasticity, may influence ultrasonic response while also highlighting the value of multi-cycle testing and high-resolution waveform analysis.

The outcomes of this study have significant implications for the development of field-deployable diagnostic systems. By demonstrating the sensitivity, repeatability, and practicality of acoustoelastic-based ultrasonic measurements, this work lays the groundwork for future integration into in-situ monitoring platforms. Such systems could be deployed in aging nuclear reactors, transportation infrastructure, or post-disaster forensic investigations to rapidly assess structural integrity without the need for invasive testing.

In summary, this report establishes a comprehensive framework for ultrasonic-based stress evaluation in embedded rebar. It integrates fundamental materials science, experimental mechanics, and signal analysis to deliver a practical, scalable solution to one of the most pressing challenges in non-destructive infrastructure assessment. The research presented here represents a critical step forward in advancing NDE technology from controlled laboratory environments to real-world applications.

The remainder of this report is organized as follows. Section 2 presents a literature review of stress measurement techniques, including ultrasonic, diffraction, and magnetic methods. Section 3 introduces the acoustoelastic effect, which forms the theoretical basis for the ultrasonic approach. Section 4 describes the experimental setup and signal processing algorithm used in this study. Section 5 discusses the results of five tensile tests performed on different rebar specimens. And finally, the conclusions section presents key takeaways, future research directions, and considerations for field deployment.

2. LITERATURE REVIEW

Residual stresses introduced during manufacturing and service play a key role in the mechanical performance of materials, influencing fatigue life, structural integrity, and failure mechanisms. Several NDE techniques have been used, especially in the past few decades, to quantify the residual stresses in structural components and materials. In particular, and in the context of this study, the measurement of internal stresses within steel rebar embedded within concrete is of interest. Herein, a literature review of three separate types of NDE methodologies used to measure and calculate the internal stress within steel rebar are summarized: (1) ultrasonic methods based on the acoustoelastic effect, (2) diffraction (i.e., neutron and X-ray) techniques, and (3) magnetic methods.

2.1 ULTRASONIC TECHNIQUE BASED ON ACOUSTOELASTIC EFFECT

2.1.1 Conventional Contact Transducer

Ultrasonic methods leverage the acoustoelastic effect, in which wave velocity changes correlate with stress in materials. Using conventional contact transducers can provide more reliable and high-sensitivity results. Early work by Tanala et al. [1] explored the use of bulk waves (longitudinal waves and shear waves) and surface waves (Rayleigh waves and subsurface longitudinal waves) to measure near-surface residual stresses in welded pipe and aluminum plate. This study introduced calibration methods to account for material anisotropy and demonstrated the applicability of ultrasonic techniques for biaxial stress characterization in complex geometries. Duquennoy et al. [2] explored the characterization of residual stresses using ultrasonic Rayleigh waves. They conducted stress measurements in three different rods using Rayleigh waves in both the longitudinal and circumferential directions with conventional piezoelectric transducers and a laser vibrometer. Results indicate that the laser ultrasonic method may be more suitable for monitoring stress variations during different stages of fabrication. Castellano et al. [3] highlighted the integration of acoustoelastic techniques with non-linear elasticity models, enabling improved stress monitoring in structural components. Their work emphasized accurate measurement techniques that are adaptable for in situ applications.

Xu et al. [4] used longitudinal critically refracted (LCR) waves to measure stress in a pipe weld joint and conducted a calibration procedure using a tension test before the experiments on the weld joint. Song et al. [5] studied different LCR wave frequencies for the stress measurement of a C-shaped pipe specimen and found that the results from 15 MHz transducers had similar stress measurements to the X-ray results. Hwang et al. [6] used LCR waves and customized LCR wave probes to measure residual stresses in rail specimens. The LCR waves were bulk longitudinal waves traveling down the surface of the material. This technique does not require the presence of two parallel surfaces, thus avoiding that geometric constraint. This study demonstrated the suitability of LCR waves for high-sensitivity stress evaluations. Zhong et al. [7] studied longitudinal for measuring axial stress in concrete and found that waves propagating parallel to the stress direction were more sensitive to axial stress than those traveling in other directions. Zeng et al. [8] investigated the sensitivity of longitudinal waves and shear waves that propagate perpendicular to the stress direction. The results showed that the shear wave with polarization parallel to the stress direction is the most sensitive, and the authors also proposed a temperature compensation technique for the temperature variations due to loading. More recently, Choi et al. [9] utilized ultrasonic minimum reflection methods with Rayleigh waves to evaluate residual stresses in shot-peened INCONEL 718. Their work provided valuable insights into stress distribution with depth and further demonstrated the versatility of ultrasonic techniques for evaluating advanced materials.

2.1.2 Laser Ultrasonic Techniques

Laser-based ultrasonic methods are a promising alternative for precise and non-contact stress evaluation. Compared to conventional contact transducers, laser ultrasonic sensing imposes no requirements for surface preparation, and the laser sensor is typically a wide-band transducer. However, when using a laser as the excitation source, its excitation energy is lower than the conventional contact transducer. He and Kobayashi [10] introduced a non-contact stress measurement technique using laser Doppler velocimetry to detect Rayleigh waves on stainless steel and aluminum samples. Their method provided a more accurate and flexible means of determining the stress–acoustic coefficient and evaluating residual stress. Karabutov et al. [11] developed optoacoustic transducers to enhance the detection of stress-induced wave variations in metallic welds as a semi-noncontact sensing method. The optoacoustic transducer used an Nd-YAG laser as the excitation source and an $LiBbO_3$ piezoelectric transducer as the receiver. The stress measured from the proposed optoacoustic transducer and longitudinal wave velocity showed consistent results with conventional techniques. Sanderson and Shen [12] demonstrated the depth profiling of stress distributions up to 0.3 mm in metals using laser-generated ultrasound. Marusina et al. [13] explored laser diagnostics for subsurface stress distribution in metals, highlighting the sensitivity of laser ultrasonics to material deformation. Zhan et al. [14] demonstrated the feasibility of using laser-generated surface waves for measuring welding residual stresses and used finite element modeling for validation.

Table 1 shows a simple summary of the wave modes used for stress measurement. Typically, longitudinal and shear waves are the most common wave modes used for stress measurement or monitoring. These two wave modes are easy to excite. However, the propagation direction and polarization direction determine the sensitivity of these two wave modes. Usually, the wave velocity has the highest sensitivity to the stress when the wave propagation and polarization direction are both parallel to the stress direction. Rayleigh waves have typically been used for surface stress measurement since they propagate without radiation loss and concentrate the energy within the depth of the one wavelength. However, a limitation of Rayleigh waves is their limited sensitivity to stress changes at greater depths. Another wave mode used is LCR wave, which is a special type of longitudinal wave that propagates along a material's surface but penetrates the bulk at shallow depth. Compared to Rayleigh waves, LCR waves may propagate deeper—from millimeters to centimeters. Their wave speed is affected by bulk stress, rather than the surface stress as is the case for Rayleigh waves. LCR waves are less affected by surface roughness, oxidation, and coatings because they propagate primarily through the material's interior. Lamb waves are typically used for stress measurement in plate-like structures, and the frequency used depends on the thickness and material of the plate. Typical frequencies for stress measurement using the above techniques range from 1 MHz to 10 MHz for metal materials. However, for special applications, a lower frequency can be used for composite materials (e.g., concrete and carbon fiber–reinforced polymer).

Table 1. Ultrasonic wave mode used in the literature for stress measurement.

Wave mode used	References
Longitudinal wave	[1], [11], [13], [7]
Shear wave	[1], [3]
Longitudinal wave and shear wave	[1], [15], [8], [16], [17]
Rayleigh wave	[1], [2], [9], [10], [14], [12]
Longitudinal refracted wave	[4], [5], [6]
Lamb wave	[18], [19], [20]

2.2 DIFFRACTION METHOD

Diffraction NDE techniques include subjecting material specimens to either neutron or X-ray beams and collecting data on the diffracted signal. Diffraction NDE methodologies are used to measure residual or applied stresses in materials with applications to bulk measurements within thick specimens. The elastic strains are determined by measuring the changes in the lattice spacings of crystalline material. The stresses are then derived using Hooke's law and assuming linear elastic behavior. A specimen is moved through either a neutron or X-ray beam, and stresses within a small volume are determined at different locations within the material [21].

When a specimen is exposed with a neutron or X-ray beam with a particular wavelength, it produces a diffraction pattern that, in turn, can be used to determine the position of each plane of the material using Bragg's law. The residual strain within a material is measured in the direction of the scattering vector; the scattering vector bisects the angle between the incident and diffracted beams and is also perpendicular to the diffracting planes within the material specimen. The lattice spacings are determined by measuring the angular positions of the diffraction peak (i.e., the Bragg reflection) by subjecting the material to either a neutron or X-ray beam [21].

2.2.1 Neutron Diffraction Method

Several studies have been conducted to determine the residual strains and stresses within steel rebar using diffraction techniques [22], [23], [24], [25], [26], [27], [28]. Many research efforts have quantified the internal states of rebar employing a pulsed-neutron powder diffractometer, the Engineering Materials Diffractometer (TAKUMI), located at the Materials and Life Science Facility in the Japan Proton Accelerator Research Complex (J-PARC) [22], [23], [24], [25]. In particular, Harjo et al. [22] summarized recent efforts at the J-PARC facility. Within this work, four separate experiments are outlined, involving: (1) the ITER (i.e., the world's largest tokamak, a magnetic fusion device) central solenoid, (2) steel rebar embedded in concrete, (3) transformation induced plasticity steel, and (4) long-period stacking ordered Mg-Zn-Y alloys. For each of these applications, the internal strains were determined and were found to be in agreement with results obtained from traditional strain gauges. In particular, for the study involving the steel rebar embedded in concrete under pull-out loading, internal strain distributions were measured at external stresses of 33 MPa, 125 MPa and 250 MPa within rebar with a 9.53 mm nominal diameter that was embedded in a cylindrical concrete measuring 50 mm in diameter and 460 mm in length [22]. Overall, the measurements related to residual strain mapping are about 24.4% of the whole beam time in TAKUMI, while various kinds of in situ measurements are 52.3%. The NDE neutron diffraction technique employing TAKUMI can be widely used in many engineering applications, such as civil infrastructure, nuclear power plants, and underground infrastructure that may experience relatively high pressures [22].

Furthermore, other NDE experiments involving steel rebar have been conducted at the J-PARC facility using TAKUMI [23], [24], [25]. Suzuki et al. [23] used TAKUMI to determine the three-dimensional deformation behavior of steel rebar embedded in normal-strength concrete that was cured in air. The methodology employed within this study was the time-of-flight (TOF) neutron diffraction method, which uses the TOF neutron diffraction to measure changes in lattice spacing. A 9.53 mm nominal diameter steel rebar was embedded in a cylindrical volume of concrete (i.e., 50 mm diameter and 460 mm length). The strain distributions were measured at 5 mm intervals along the rebar over the length of 300 mm, under different pull-out loadings (i.e., approximately 33, 125, and 250 MPa). A strain gauge fixed on the external region of the rebar verified that the rebar did not yield during the experiment. Finally, Hooke's law was applied to determine the stress distributions along the rebar; axial and lateral stresses were reported in the range of approximately 0–300 MPa. Overall, this study was able to determine stresses along steel rebar embedded within concrete at a relatively fine resolution. However, this type of

experiment could not be conducted on-site at a nuclear power plant; a specimen must be extracted and brought to the laboratory facilities to be subjected to the TAKUMI instrumentation [23].

Suzuki et al. [24] also employed TAKUMI at the J-PARC facility to conduct neutron diffraction experiments on steel rebar embedded in concrete. Within this work, the TOF neutron diffraction technique was used to determine the bond deterioration associated with damage such as cracks and corrosion in the reinforced concrete. Two separate experiments were carried out to determine: (1) the stress measurement along a rebar around cracks in concrete and (2) the stress distribution along a corroded rebar embedded in concrete. For the cracking experiment, a 12.7 mm nominal diameter steel rebar was embedded in a rectangular-shaped concrete specimen with dimensions of 400 mm in length, 100 mm in height, and 50 mm in width. The strain distributions were measured along the rebar during tensile loadings at approximately 10, 75, and 150 MPa; Hooke's law was applied, and axial stress ranges of 0–150 MPa were observed. For the corrosion experiment, a steel rebar with 9.53 mm in nominal diameter was embedded in a cylindrical concrete with 51 mm diameter and length of 460 mm. Three separate specimens with different corrosion rates, including one with no corrosion, were prepared for this experiment. The strain distributions were measured along the rebar during pull-out loadings at approximately 30, 125, and 250 MPa. For the corrosion study, a range of 0–250 MPa axial stress was reported [24].

The final study using TAKUMI reviewed herein, Suzuki et al. [25], conducted an experiment involving the neutron diffraction technique with high spatial resolution to investigate local bond resistance caused by the transverse ribs of steel rebar embedded in concrete. The purpose of this study was to evaluate the bond condition of reinforced concrete based on the bond stress distribution along the embedded rebar. In this experiment, a steel rebar with a nominal diameter of 9.53 mm was embedded in a cylindrical volume of concrete measuring approximately 50 mm in diameter and 460 mm in length. Strain measurements were collected at 5 mm increments along the rebar. Using Hooke's law, axial and bond stresses were derived along the bar; the average error bar of the measured axial stresses was ±22 MPa [25].

The rebar experiments conducted at J-PARC with TAKUMI [23], [24], [25] have demonstrated that the TOF neutron diffraction technique is suitable for determining residual stresses in steel rebar embedded within concrete. This NDE methodology can effectively permeate a layer of concrete to derive structural and material information regarding the steel rebar. However, a major limitation of this technology is that it is presently not portable and therefore cannot be deployed in the field. In order to determine stresses in rebar in situ, a sample would need to be destructively removed from the structure and transported to a facility to be further tested.

Another experiment conducted at J-PARC using RADEN, an energy-resolved neutron imaging instrument using pulsed neutrons, is summarized in Koyama et al. [26]. Using the RADEN equipment, it is possible to visualize the spatial distribution of various quantities concerning crystallographic structure, elemental concentration, temperature, magnetic field, and typical neutron radiography and tomography. Within this work, a novel method was developed that observes the internal deformation of concrete using neutron transmission imaging techniques and a lattice method. To visualize the internal deformation of concrete, cement paste markers containing gadolinium oxide powder were dispersed two-dimensionally around steel rebar in reinforced concrete. Displacement of the neutron transmission image of the gadolinium oxide markers was evaluated by tracking changes in marker position as a function of the vertical sample stage's travel distance. This study examined a steel rebar with a nominal 12.7 mm diameter that was embedded in a rectangular concrete specimen 50 × 50 × 130 mm in size. Full strain imaging was achieved using this NDE methodology. Overall, this technique is not feasible for in-field measurements because the gadolinium oxide needs to be dispersed into the specimen. The instrument used to perform the neutron imaging is located within a facility, and a portion of the rebar would need to be transported to this facility for testing [26].

In addition to the experiments conducted at J-PARC, another rebar study was carried out using the diffractometer for residual stress analysis at the Japan Research Reactor No. 3 of the Japan Atomic Energy Agency, as outlined in Yasue et al. [27]. In this study, the relationship between measurement time and accuracy was investigated for reinforced concrete specimens with different cross-sectional shapes, measurement positions, and cover thicknesses to determine the accuracy of the measurements using neutron diffraction methods. The change in lattice spacing of a material when a load is applied to the material can be translated into a change in the diffraction angle. The elastic strain is then calculated by measuring the change in diffraction angle. For this experiment, the specimens were prepared by placing a 400 mm long rebar in concrete with five different cross-sectional shapes within concrete over a length of 260 mm. Although strain measurements were derived from this experiment, they were not converted to stress and were determined only at discrete points along the rebar. In summary, this methodology cannot be replicated in the field and would, again, require that a sample be taken from the field in a destructive manner and transported to a laboratory facility for further testing and experimentation [26].

2.2.2 X-Ray Diffraction Method

Although neutron diffraction is more widely used in experimental studies, X-ray diffraction is also employed to achieve similar results of stress and strain measurements within rebar samples. For example, Yanagida et al. [28] used X-ray diffraction to measure residual stresses in steel bars and analyzed how steel strength affects the accuracy of internal stress measurements. They found that for ordinary steel bars with yield strengths of approximately 550 MPa or lower, the X-ray residual stress measurement values tended to be lower than the actual stress values from the point at which a loading stress of approximately 40% of the yield strength was generated. Furthermore, the X-ray stress measurements at the point when the stress in the rebar reached its yield strength were about 70% to 80% of the actual stress. Additionally, to accurately measure the residual stress of rebar with a yield strength of 1000 MPa or higher, the measurement points must be electropolished in advance. Therefore, for high-strength steel rebar, it would be necessary to prepare the samples in advance to use this measurement technique. Because of this limitation and the fact that the rebar studied in these experiments was not embedded in concrete, this methodology would not be suitable for field deployment in civil infrastructure or at nuclear power plants [28].

2.3 MAGNETIC METHOD

The third general NDE methodology reviewed herein is magnetic methods. In theory, magnetic methods for NDE of residual stresses can be rapidly deployed and used in situ on structural components. This NDE method can be applied to ferromagnetic materials like steel rebar embedded in concrete. This technique relies on using a probe that applies an alternating magnetic field to the specimen surface and sensors that monitor electromagnetically induced voltages in the specimen. These sensors may measure a wide array of different magnetic properties and their correlation to the microstructural features and material properties like hardness and residual stress. Herein, several literature studies are reviewed that have used magnetic methods to measure internal conditions within steel rebar [29], [30], [31].

Tong et al. [29] aimed to measure the stress state of steel rebar under different applied magnetic field excitations, using graded weak magnetic excitation. The purpose of this study was to find a quantitative relationship between the strength of the field of excitation, magnetic signal, and tensile load of the rebar, in addition to quantitatively measuring the internal stresses of the rebar. The general methodology of the experiment was to subject magnetic field excitation to rebar samples and then measure changes in magnetic properties. The magnetic field was then used to calculate residual stress using empirical relationships. The algorithm used to determine the stress calculation equation is complex and requires many human inputs and interpretations; however, once this empirical equation is established, the quantitative measurement of the stress state of rebar in the elastic stage may be achieved. The instruments

used in this experiment include an electro-hydraulic servo universal testing machine, a three-dimensional spontaneous magnetic flux leakage (SMFL) collector, a high-precision DC power supply, and a copper wire solenoid. The three-dimensional SMFL collector consists of a magnetic sensor, a serial server, and a PC terminal. Because this experimental setup is situated within a laboratory environment, the portability of such equipment to the field is questionable, and, therefore, the application of this technique to in situ structures may not be practical. Furthermore, because of the complex nature of determining the empirical stress equations quantifying the relationship between magnetic signal and internal stress and the fact that human intervention and interpretation are required at multiple steps in this process, this NDE technique has severe limitations and most likely could not be rapidly deployed.

Xia et al. [30] used magnetic NDE methods to monitor the working stress of rebars. A novel magnetic resonance sensor was used in this study to carry out experimental research. The correlation between rebar stress and the sensor's induced voltage was theoretically analyzed using the magnetoelastic effect and magnetic resonance theory. A working stress monitoring method for prestressed rebars based on magnetic resonance was proposed. This paper combined the magnetoelastic effect, electromagnetic induction law, and magnetic resonance effect. First, the relationship between sensor-induced voltage and rebar stress was analyzed. Then, working stress monitoring experiments under different working conditions were carried out on steel rebars with different diameters (i.e., 16, 18, and 20 mm diameters). Finally, the nonlinear relationship between the induced voltage peak-to-peak values and the prestress was analyzed. Although internal stresses were able to be derived from the magnetic experiments with an average relative error value of less than 15%, the procedure to calculate the stresses involves several curve-fitting processes with human involvement and discernment for calibration. Furthermore, this experiment did not include rebar embedded within concrete and relied on surface-level measurements that were collected at discrete points along the rebar. Because of these limitations and the fact that these experiments are conducted within a laboratory environment with non-portable equipment, this methodology would not be suitable for use in the field to measure residual stress of steel rebar embedded within concrete.

Lastly, Zhou et al. [31] examined the quantitative evaluation of rebar stress based on weak magnetic effect in a similar fashion as Xia et al. [30]. In this work, the weak magnetic detection method was used to characterize the internal stress of rebar. A stress measurement method based on the characteristic parameters of the force–magnetic coupling was proposed. The stress evaluation and classification of the rebar were completed through a combination of experimental analysis, numerical simulation, and the Bayesian classification method. Using a similar experimental setup as Xia et al. [30], internal stress within steel rebar, not embedded within concrete, was determined. The novel use of Bayesian classification techniques within the quantitative algorithm to calculate internal stresses makes this approach interesting and promising. However, the rebar tested within this work was not embedded in concrete, indicating that this methodology relies on surface-level measurements. In a field application, it is not always easy or practical to gain access to the surface of steel rebar; a sample of the rebar would need to be destructively extracted and sent to a facility for further testing and analysis. Because of these limitations, this magnetic NDE method may not be well suited to measuring steel rebar within aged civil infrastructure or nuclear power plants [11].

Table 2. Comparison of different methods for stress measurement.

Methods	Ultrasonic method	Neutron diffraction	X-ray diffraction	Magnetic method
Basic principle	Based on the acoustoelastic effect	The lattice spacings are derived using the measurements of angular positions of the diffraction peak	Same as neutron diffraction but with X-ray beam instead	Based on the magnetoelastic effect
Material Types	Metal, composite, concrete	Metal material	Metal material	Ferromagnetic materials
Accuracy	± 5–40 MPa	± 10–20 MPa	± 5–15 MPa	± 10–30 MPa (with calibration)
Measurement depth	Depends on the wave modes and frequency	10 mm to several cm	5–50 μm	~ 0.1–1 mm
Limitation	Calibration needed, results affected by the surface roughness and temperature	Large and expensive facility required	Shallow penetration depth, requires crystalline materials	Only for ferromagnetic Materials, calibration needed
Field Applicability	Can be used for field testing	Facility equipment	Portable machine	Fast and portable
Cost	Low	High	Medium	Low

3. ACOUSTOELASTIC EFFECT

The *acoustoelastic effect* refers to the phenomenon in which the velocity of ultrasonic waves propagating through a material varies as a function of applied stress or strain. This behavior arises due to the nonlinear elastic properties of solids, where the stress state alters the stiffness of the material and, consequently, the acoustic wave speed. In the linear elastic range, the relationship between stress and ultrasonic velocity is typically approximated as linear, particularly for longitudinal and shear wave modes. The foundational theory was first described by Hughes and Kelly in the 1950s [32] and has since been applied extensively in NDE, particularly for residual stress and in situ stress measurements in metals, concrete, and composites. For isotropic media submitted to uniaxial loading in direction 1, as shown in Figure 1, the velocities of elastic waves are expressed as follows:

$$
\begin{aligned}
\rho_0 V_{11}^2 &= \lambda + 2\mu + \frac{\sigma_{11}}{3K}\left[\, 2l + \lambda + \frac{\lambda+\mu}{\mu}(4m + 4\lambda + 10\mu)\,\right] \\
\rho_0 V_{12}^2 = \rho_0 V_{13}^2 &= \mu + \frac{\sigma_{11}}{3K}\left[m + \frac{\lambda n}{4\mu} + 4\lambda + 4\mu\right] \\
\rho_0 V_{22}^2 = \rho_0 V_{33}^2 &= \lambda + 2\mu + \frac{\sigma_{11}}{3K}\left[2l - \frac{2\lambda}{\mu}(m + \lambda + 2\mu)\right] \\
\rho_0 V_{21}^2 = \rho_0 V_{31}^2 &= \mu + \frac{\sigma_{11}}{3K}\left[m + \frac{\lambda n}{4\mu} + \lambda + 2\mu\right] \\
\rho_0 V_{23}^2 = \rho_0 V_{32}^2 &= \mu + \frac{\sigma_{11}}{3K}\left[m - \frac{\lambda+\mu}{2\mu} n - 2\mu\right]
\end{aligned}
\tag{1}
$$

In the equations, (l, m, n) are Murnaghan's constants and (λ, μ) are Lamé's coefficients. ρ_0 is the density of the material and $K = \lambda + \frac{2}{3}\mu$ is the compressibility modulus. V_{ij} represents the velocity of the wave propagating in direction i and polarized in direction j, and σ_{11} is the normal stress in direction 1. When performing the linearization of Equation (1) at the first order, the velocity can be expressed as a linear function of the stress applied:

$$
V_{ij}^{\sigma} = V_{ij}^{0}\left(1 + A_{ij}\sigma_{11}\right), \tag{2}
$$

where the V_{ij}^0 is the velocity at zero stress, and V_{ij}^{σ} is the velocity at the stress of σ_{11}.

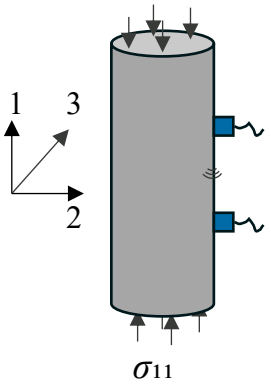

Figure 1. Diagram for stress and wave propagation directions on an isotropic rod.

In practice, the acoustoelastic effect is influenced by several factors, including material anisotropy, temperature, microstructural state, and strain rate. Temperature in particular has a direct effect on ultrasonic wave velocity due to thermal expansion and softening of the elastic modulus. Therefore, accurate stress measurement using the acoustoelastic effect often requires compensation for temperature fluctuations. Additionally, the strain rate can influence the stress state during dynamic loading, though its effect is generally minimal in quasi-static tests. By leveraging the acoustoelastic effect, ultrasonic techniques can provide a noninvasive and repeatable means to monitor stress evolution in structural materials, making it a valuable tool for applications such as rebar stress evaluation in nuclear concrete structures.

4. EXPERIMENTAL SETUP AND SIGNAL PROCESSING ALGORITHM

4.1 EXPERIMENTAL SETUP FOR TENSILE TEST AND ULTRASONIC MONITORING

4.1.1 Rebar Tensile Test

The test rebar measured 16 in. in length and 1 in. in diameter. Prior to tensile testing, two ultrasonic transducers were mounted on the polished surface of the rebar using epoxy. The transducers were positioned 3 in. apart at the center of the rebar. A type-T thermocouple was affixed at the midpoint between the two transducers to monitor temperature. As shown in Figure 2, the tensile grips engaged 3.75 in. of the rebar at each end. An 8 in. extensometer was installed outside the region between the ultrasonic transducers to measure axial strain. During the tensile test, load and strain data were recorded in parallel with ultrasonic signals and temperature measurements.

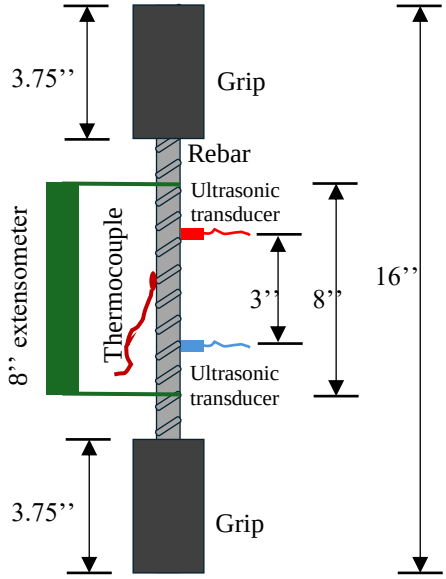

Figure 2. Experimental test setup for rebar tensile test and transducer installation.

Testing was performed in a custom-built 200 kip servo-hydraulic MTS mechanical test frame equipped with 647 Hydraulic Wedge Grips (MTS Systems, Eden Prairie, MN). The sample was outfitted with an axial 1 in. extensometer with a 7 in. extension and secured with rubber bands. Samples were gripped with 6000 psi and loaded in both tension and compression under a load-controlled protocol at a rate of 50 lb/s to 100 lb/s. Data were collected at a rate of 10 data points per second using an in-house LabView program.

4.1.2 Ultrasonic Monitoring Setup

Ultrasonic signals were acquired using a customized ultrasonic measurement system, as illustrated in Figure 3. A 5 MHz ultrasonic transducer was used as the transmitter and was excited by a pulser–receiver unit (DPR500, BYK-Gardner, Pittsford, NY). The ultrasonic waves propagated through the rebar and were captured by a receiving transducer. The received signals were amplified by the pulser–receiver and digitized using an oscilloscope (Picoscope 5444D MSO, Pico Technology, Cambridgeshire, UK) at a sampling rate of 12.5 MS/s. To improve the signal-to-noise ratio, each waveform was averaged over 100 acquisitions. Simultaneously, the temperature of the rebar was monitored using a type-T thermocouple

connected to a temperature logger (NI-9211, National Instruments). Both ultrasonic and temperature data were recorded every 5 s throughout the tensile test. Data acquisition was fully automated and controlled via a custom LabVIEW program.

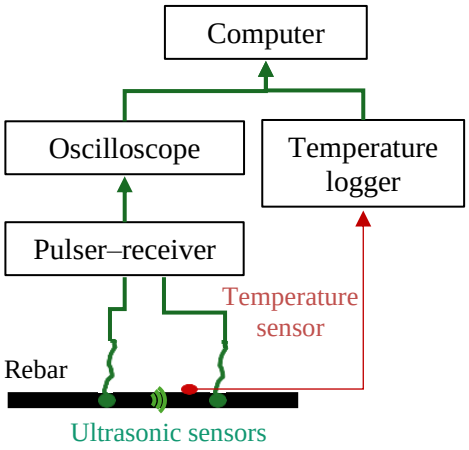

Figure 3. Schematic for rebar tensile test and transducer installation.

4.2 Signal Processing Algorithm

According to the literature, the relative velocity change is on the order of 10^{-5} /ksi for common metal materials (e.g., aluminum, steel). Such a small velocity change cannot be detected by measuring the direct arrival time. Coda wave analysis techniques are used to track the ultrasonic velocity change due to the temperature change. The stretching technique was first proposed by Lobkis and Weaver [33]; the method allows processing the full waveform by applying a stretching factor ε to the perturbed signal φ'. Using the stretching technique, the cross-correlation coefficient CC is evaluated as

$$CC(\varepsilon) = \frac{\int_{t_1}^{t_2} \varphi'[t(1-\varepsilon)]\varphi[t]dt}{\int_{t_1}^{t_2} \varphi'^2[t(1-\varepsilon)]dt \int_{t_1}^{t_1} \varphi^2[t]dt} \quad (3)$$

In this equation, the stretching factor ε, which maximizes the cross-correlation coefficient, represents the relative velocity change dv/v.

Figure 4 shows the time-domain signals at the rebar stress of 1 ksi (blue) and 25 ksi (red). In the coherent wave part, the phase difference between the two signals is small. However, in the coda wave part (320 μs to 360 μs), there is a large phase difference between the two signals. In this work, the window [320, 360] μs was used to calculate the relative velocity change between two signals. Figure 5 plots the cross-correlation coefficients at different stretching factors. When the cross-correlation coefficient reaches the maximum, the stretching factor is -7.72×10^{-4}, which is the relative velocity change between the two signals. Initially, the first time-domain signal was used as the reference signal, and all the other signals were compared to the reference signals to calculate the relative velocity change. Once the correlation coefficient is lower than a threshold value (e.g., 0.95), the current signal is used as the new reference. More details can be found in Sun [34].

The relative velocity change determined using the stretching technique is then used to derive the slope *k*, which quantifies the sensitivity of ultrasonic velocity to applied stress. This slope, expressed in units such as 1/ksi, is a key parameter for evaluating the acoustoelastic response of the material. Consistency of this slope across different tests indicates the robustness and repeatability of ultrasonic measurements and serves as a benchmark for comparing field and laboratory measurements.

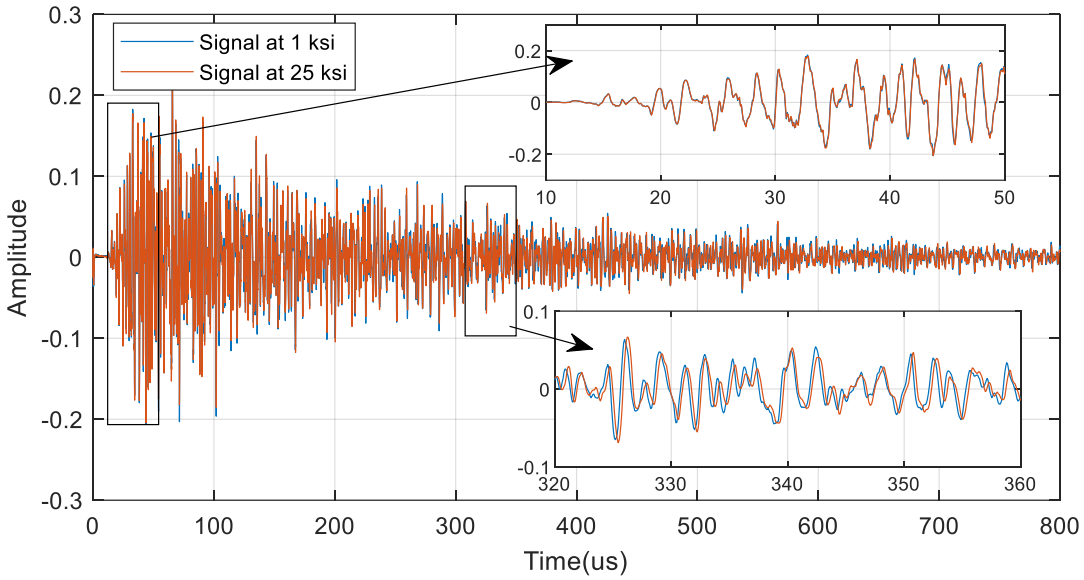

Figure 4. Time-domain signals at 1 ksi and 25 ksi.

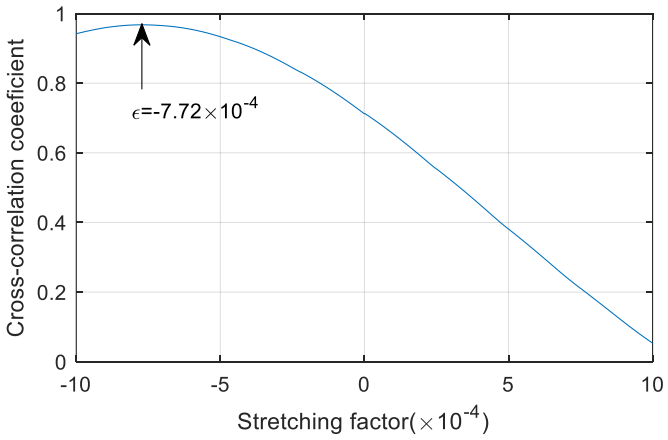

Figure 5. Cross-correlation coefficient at different stretching factors.

5. RESULTS

Tensile tests were conducted on four different #8 rebars with a diameter of 1 in. and one #6 rebar with a diameter of ¾ in. The testing conditions for these rebars are summarized in Table 3.

Table 3. Summary of the rebar tensile testing.

Index	Size #	Diameter	Yield (ksi)	Maximum load (kips)	% yield stress	Load/unload cycles
1	8	1”	60	27	57.3	1
2	8	1”	60	33	70	1
3	8	1”	60	42	89.1	4
4	8	1”	60	52	110	3
5	6	¾”	60	18	68	2.5

5.1 TEST 1: #8 REBAR WITH 57% YIELD STRESS

In the initial test, the rebar was loaded up to 27 kips, corresponding to a maximum tensile stress of 34.4 ksi, which is approximately 57.3% of the material’s yield strength (60 ksi). Figure 6(a) illustrates the loading profile over time. The linear loading rate is about 24.8 lb/s. The rebar was initially loaded to the peak load and then unloaded to zero. Since the loading was displacement-controlled, a nonlinear (curved) load-time response appeared after approximately 1500 s. Figure 6(b) presents the stress–strain curve for this test, which shows a clear linear relationship, indicating elastic behavior. The slope of this curve represents the elastic modulus of the material, which was measured to be 288 GPa for this sample.

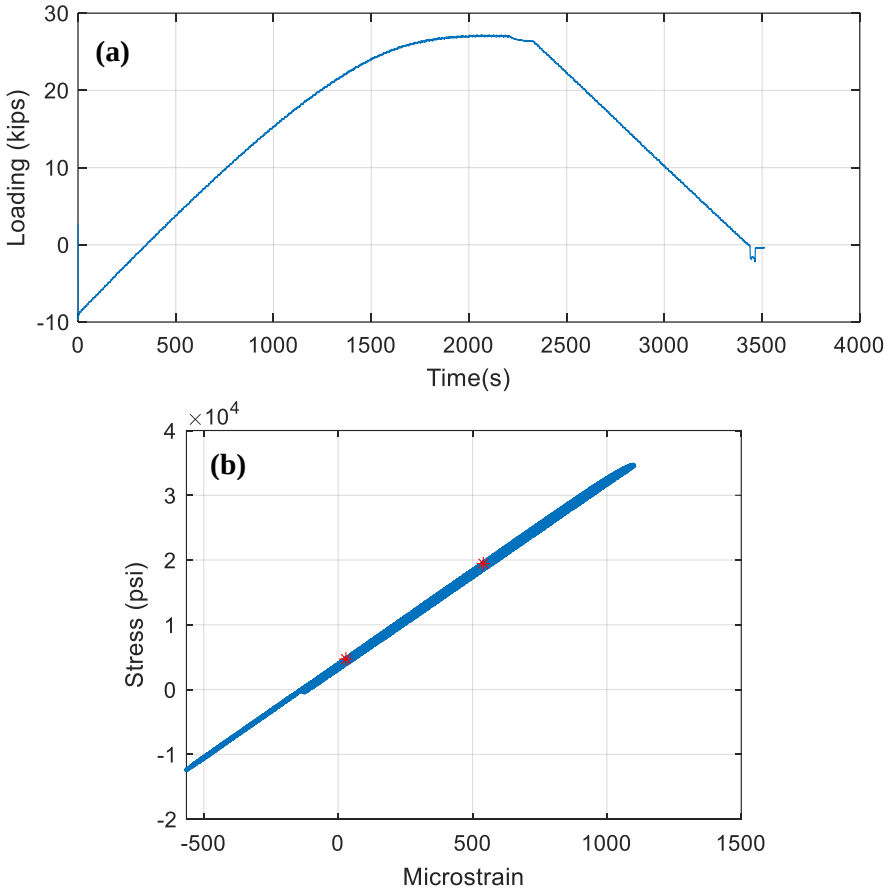

Figure 6. (a) Load profile for the rebar in test 1 and (b) stress–strain curve for test 1.

Figure 7 shows the time history curves of stress (load), temperature, and the corresponding ultrasonic velocity during both the loading and unloading phases. A slight decrease in temperature was observed during loading, followed by an increase during unloading. This behavior is attributed to the thermoelastic effect [35]. When a material undergoes elastic deformation, such as during tensile loading, its internal energy is redistributed. In the elastic regime, the material absorbs mechanical energy, resulting in a temporary temperature drop. Upon unloading, the stored energy is released, leading to a temperature rise. As expected, the ultrasonic velocity decreased during loading and increased during unloading; this result is consistent with stress-induced changes in elastic properties. Between 2300 s and 2600 s, the ultrasonic velocity exhibited significant fluctuations due to unstable load-holding conditions during that interval.

As shown in Figure 8, the applied load was first converted to stress, and the stress was then correlated with the measured ultrasonic velocity. A linear relationship was observed between stress and ultrasonic velocity in both the loading and unloading phases. The linear regression fits for both phases yielded high coefficients of determination (R^2), indicating strong linear correlations. The slope of the linear relationship was fitted, which represents the sensitivity of the ultrasonic velocity change per unit stress (ksi). During the loading phase, the slope was $k = -1.86 \times 10^{-5}$ /ksi, whereas the slope was $k = -2.44 \times 10^{-5}$ /ksi during unloading. The difference in slopes between loading and unloading may be attributed to the displacement-controlled nature of the loading process and the presence of residual manufacturing stress in the rebar during loading.

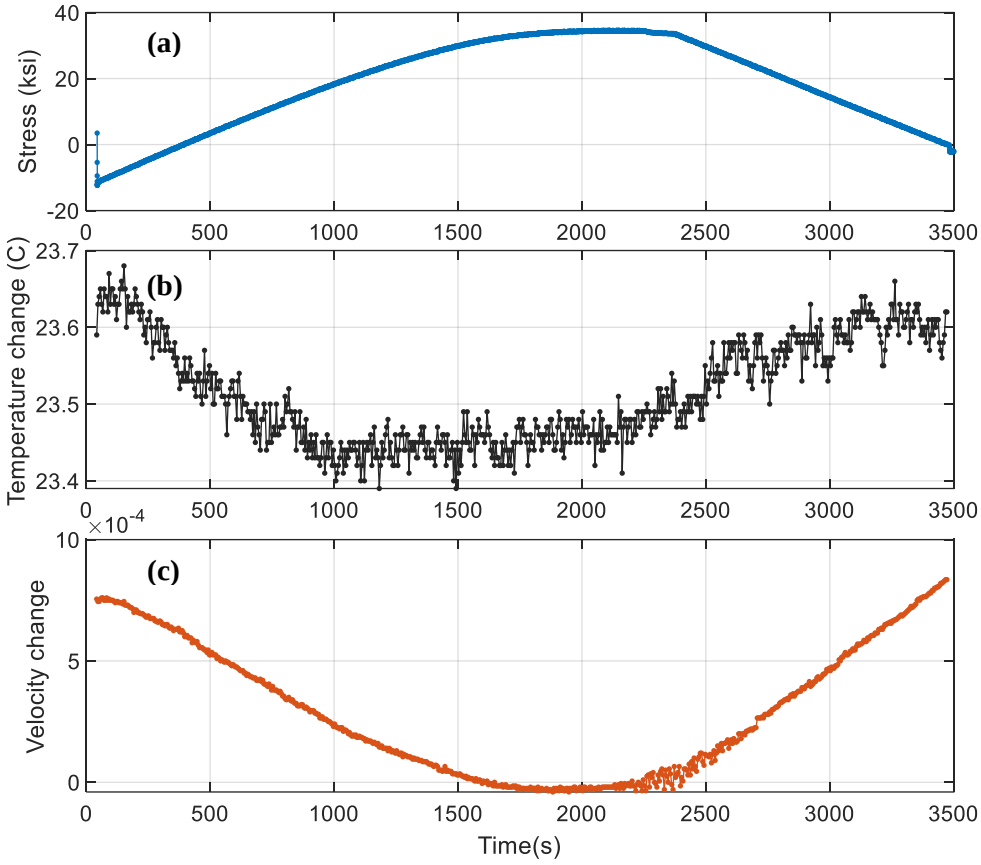

Figure 7. Test 1: (a) Stress history, (b) temperature history, and (c) ultrasonic velocity history.

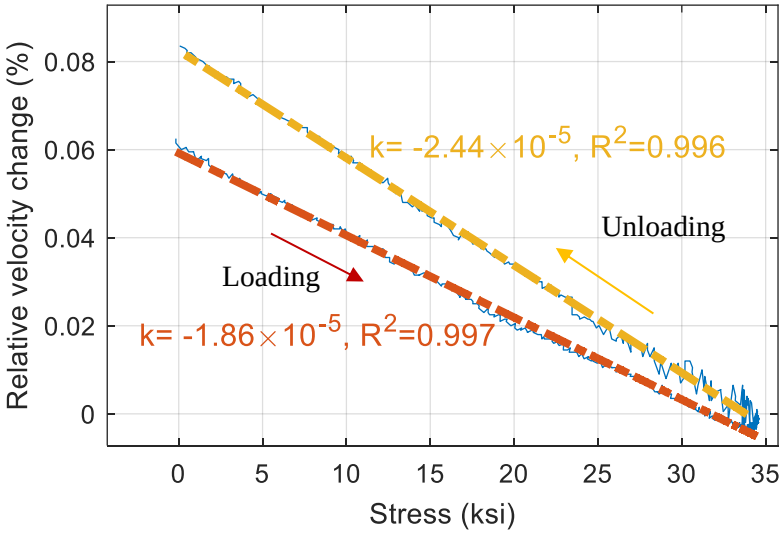

Figure 8. Test 1: Correlation between rebar tensile stress and ultrasonic velocity.

5.2 TEST 2: #8 REBAR WITH 70% YIELD STRESS

In the second test, the rebar was loaded to 70% of its yield stress using a force-controlled loading pattern. The loading rate was 50 lb/s, which was about two times that used in Test 1. The stress history is shown in Figure 9(a). Figure 9(b) presents the temperature history, which exhibits a decrease during loading and an increase during unloading; this is consistent with the thermoelastic effect. The corresponding ultrasonic velocity history during the loading process is shown in Figure 9 (c). At approximately 251 s, a sudden increase in velocity was observed, which is attributed to the closing of the top grip on the testing machine. Around 550 s, the velocity began to decrease as loading progressed, and then increased during unloading, as expected from stress-velocity coupling. At 666 s, a minor grip slip occurred due to a malfunction in the hydraulic system, which is clearly reflected in the stress history. This event also appeared as a small deviation in the velocity curve, demonstrating the high sensitivity of ultrasonic velocity measurements to subtle changes in loading conditions.

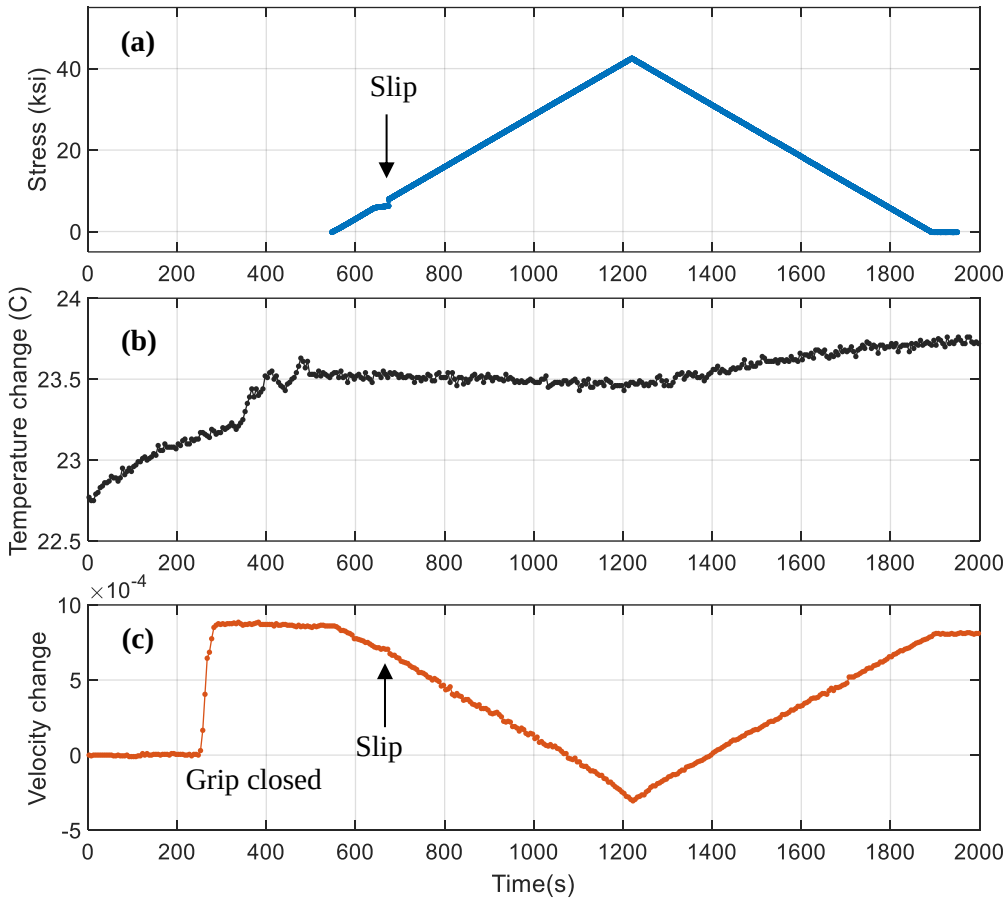

Figure 9. Test 2: (a) Stress history, (b) temperature history, and (c) ultrasonic velocity history.

Figure 10 shows the correlation between rebar stress and ultrasonic velocity. Strong linear relationships were observed in both the loading and unloading phases. The slope of the linear fit during loading was $k = -2.67 \times 10^{-5}$ /ksi, whereas during unloading it was $k = -2.55 \times 10^{-5}$ /ksi. These two slopes are very similar, likely due to the use of force-controlled loading and the minimal temperature variation between the loading and unloading phases. Notably, both slopes are also close to the unloading slope observed in Test 1, further supporting the repeatability of the stress–velocity relationship under consistent loading conditions.

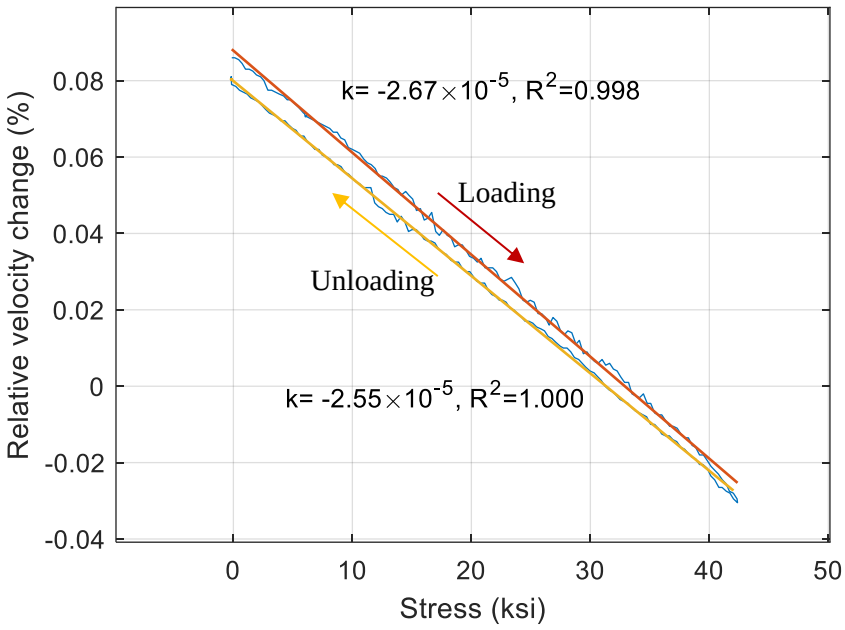

Figure 10. Test 2: Correlation between rebar tensile stress and ultrasonic velocity.

5.3 TEST 3: #8 REBAR WITH 90% YIELD STRESS AND MULTIPLE LOADING CYCLES

In Test 3, four loading–unloading cycles were conducted at a constant rate of 50 lb/s with a maximum load of 90% of the yield load. The stress history is shown in Figure 11(a). During each cycle, the load was held at the maximum and minimum stress levels for approximately 60–120 s. Figure 11(b) and 11(c) display the corresponding temperature and ultrasonic velocity histories, respectively. The correlation between stress and ultrasonic velocity for each cycle is presented in Figure 12.

With the exception of the first loading cycle, the stress–velocity curves for both the loading and unloading phases exhibited consistent linear behavior across all cycles. Linear regression slopes for each phase are summarized in Table 4. Two key observations can be made based on the results.

1. **Loading vs. Unloading Slopes:** In all cycles, the slope during loading was slightly larger in magnitude than that during unloading; this trend was also observed in Test 2. Although the slopes should theoretically be identical, the differences could be attributed to temperature variations from the thermoelastic effect and slight differences in strain rate between loading and unloading.

2. **Slope Values:** The loading-phase slopes were consistently around -2.75×10^{-5}/ksi, except in the first cycle, likely due to residual manufacturing stress. Unloading-phase slopes were approximately -2.65×10^{-5}/ksi, with the exception of the third cycle, where abnormal velocity fluctuations near 5577 s affected the result.

Overall, the results confirm the repeatability of the cyclic test and reinforce the strong linear relationship between rebar stress and ultrasonic velocity.

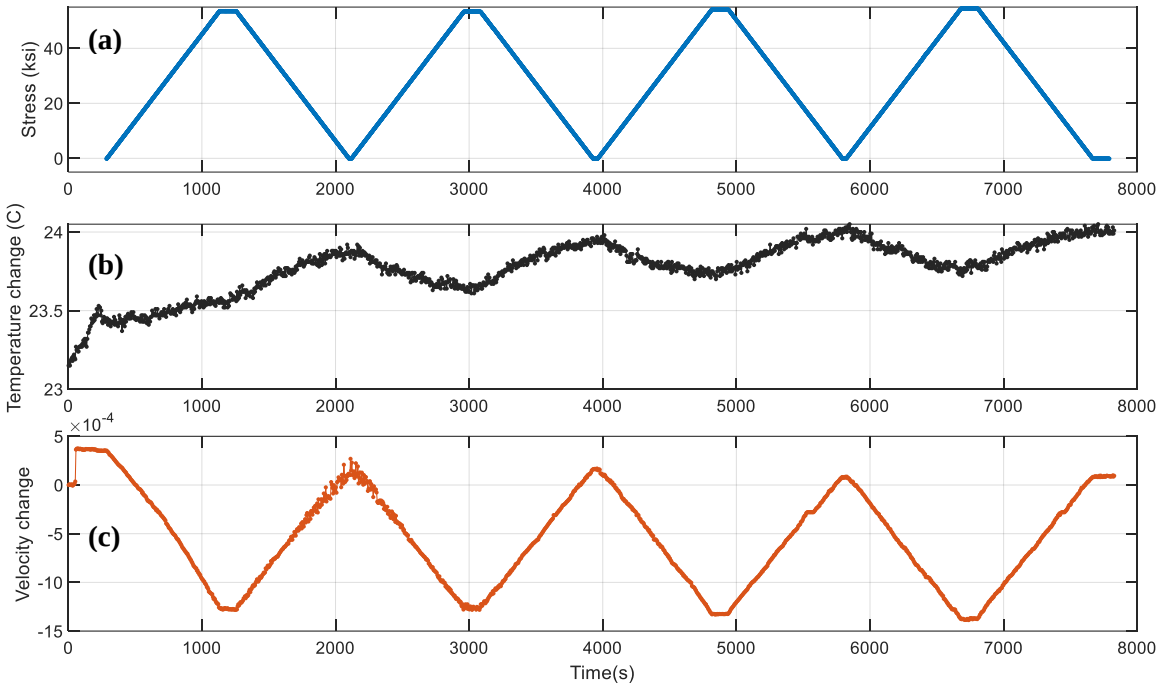

Figure 11. Test 3: (a) Stress history, (b) temperature history, and (c) ultrasonic velocity history.

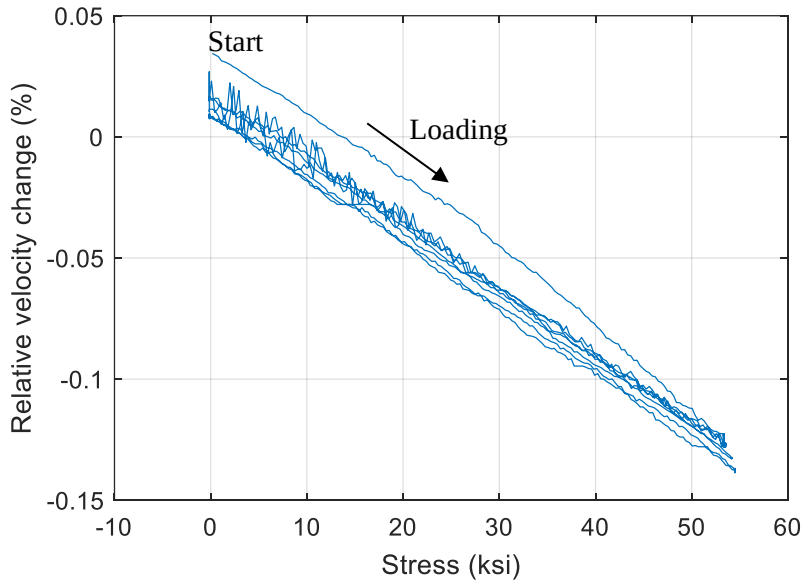

Figure 12. Test 3: Correlation between rebar tensile stress and ultrasonic velocity.

Table 4. Summary of the correlation slopes of tensile stress and ultrasonic velocity in Test 3.

Cycle	Load/unload	Slope
1	Loading ↑	$\mathbf{-2.99}\times10^{-5}$/ksi
	Unloading ↓	-2.64×10^{-5}/ksi

2	Loading ↑	-2.76×10^{-5}/ksi
	Unloading ↓	-2.68×10^{-5}/ksi
3	Loading ↑	-2.76×10^{-5}/ksi
	Unloading ↓	-2.57×10^{-5}/ksi
4	Loading ↑	-2.74×10^{-5}/ksi
	Unloading ↓	-2.64×10^{-5}/ksi

5.4 TEST 4: #8 REBAR WITH 110% YIELD STRESS AND A HIGHER LOADING RATE

In Test 4, the rebar was subjected to two initial loading–unloading cycles up to 90% of its yield stress, using a faster loading rate of 100 lb/s. In the third cycle, the load exceeded the yield point, reaching 110% of the yield stress. The load history is shown in Figure 13, where the yield load is identified as 47.1 kips. During the third loading cycle, the testing machine's grip failed at 51.0 kips, leading to the premature termination of the test. As a result of the grip failure, the ultrasonic sensor coupling was lost, rendering ultrasonic measurements unusable beyond that point. Therefore, ultrasonic velocity was only calculated up to the failure event.

Figure 14 presents the corresponding stress, temperature, and ultrasonic velocity histories. Despite approaching the yield limit, the ultrasonic velocity remained linearly correlated with stress until the point of failure. Figure 14 shows the stress–velocity correlations, and linear regression slopes for each loading and unloading segment are summarized in Table 5.

The first loading cycle exhibited a relatively large slope, consistent with observations in previous tests. The subsequent cycles displayed consistent slope values around -2.75×10^{-5}/ksi, closely matching those from earlier tests. These results further validate the repeatability of the acoustoelastic effect up to near-yield conditions and confirm the strong linear relationship between tensile stress and ultrasonic velocity.

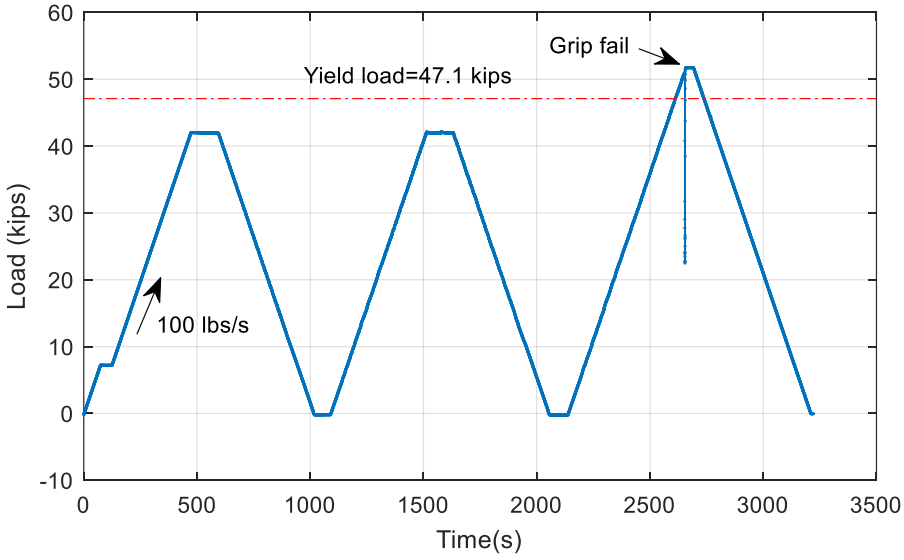

Figure 13. Test 4: Load history.

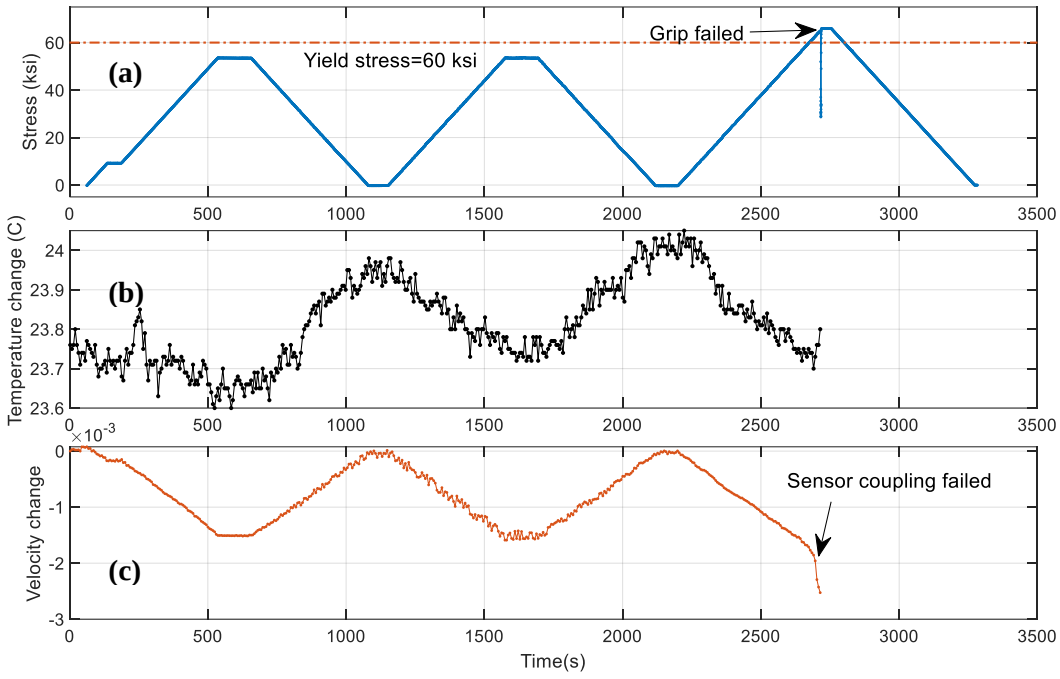

Figure 14. Test 4: (a) Stress history, (b) temperature history, and (c) ultrasonic velocity history.

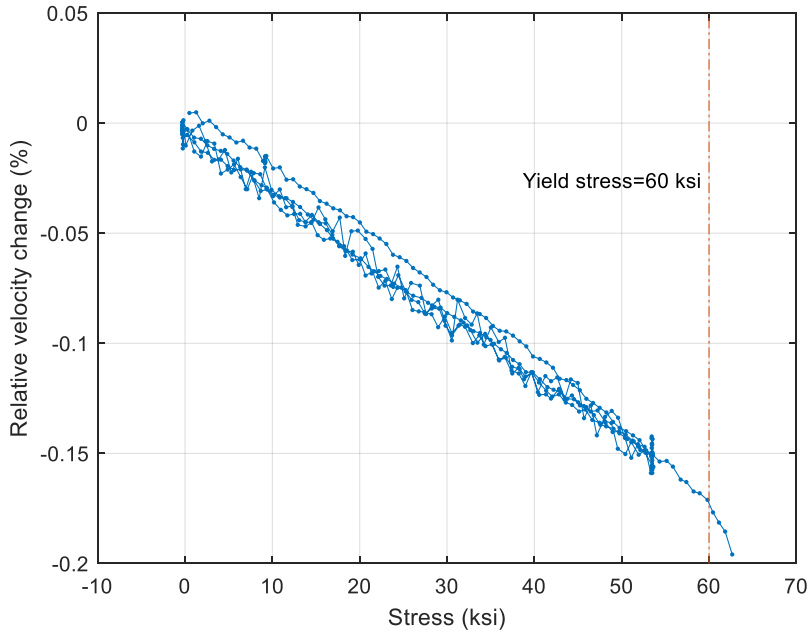

Figure 15. Test 4: Correlation between rebar tensile stress and ultrasonic velocity.

Table 5. Summary of the correlation slopes of tensile stress and ultrasonic velocity in Test 4.

Cycle	Load/unload	Slope
1	Loading ↑	-2.91×10^{-5}/ksi
	Unloading ↓	-2.77×10^{-5}/ksi
2	Loading ↑	-2.75×10^{-5}/ksi
	Unloading ↓	-2.74×10^{-5}/ksi
3	Loading ↑	-2.77×10^{-5}/ksi
	Unloading ↓	N/A

5.5 TEST 5: #6 REBAR WITH 68% YIELD STRESS

In this test, #6 Grade 60 rebar was loaded to 68% of its yield stress at a rate of 50 lb/s. Figure 16 presents the stress and ultrasonic velocity histories. The rebar underwent two complete loading–unloading cycles, reaching a maximum stress of 40.8 ksi. During the third loading cycle, the test was interrupted due to grip failure at approximately 2807 s, and the experiment was terminated at that point.

Figure 17 shows the correlation between stress and ultrasonic velocity. An approximately linear relationship was observed throughout the valid data range. Linear regression slopes were extracted for each loading and unloading segment, as shown in the figure. The slopes ranged from -2.66×10^{-5}/ksi to -2.79×10^{-5}/ksi, excluding the slope for the third loading cycle, which was affected by grip instability. These slope values are consistent with those observed in previous tests, further confirming the repeatability and linearity of the acoustoelastic response in rebar under tensile loading.

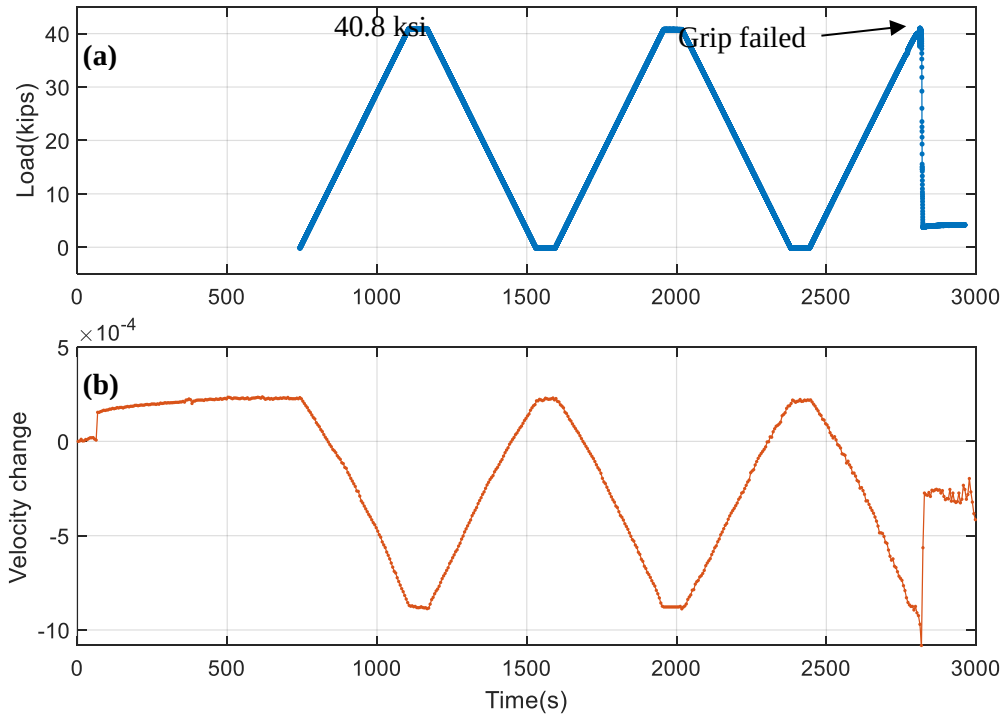

Figure 16. Test 5: (a) Stress history and (b) ultrasonic velocity history.

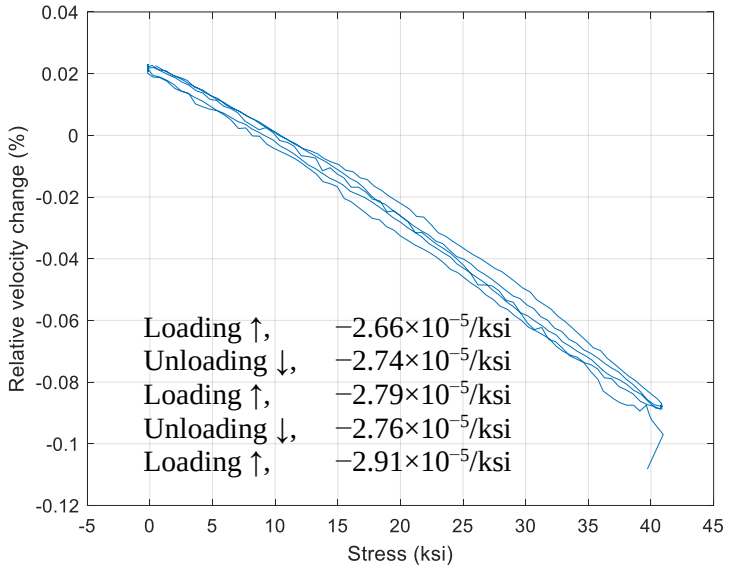

Figure 17. Test 5: Correlation between rebar tensile stress and ultrasonic velocity.

5.6 SUMMARY OF ALL TESTS

Table 6 summarizes the results and corresponding test conditions for all experiments. With the exception of the first test, the remaining tests exhibited consistent sensitivity of ultrasonic velocity to stress changes, regardless of the maximum applied stress or loading rate (50 lb/s or 100 lb/s). While the slope $\boldsymbol{k}$ (representing the velocity–stress sensitivity) remained within a narrow range across tests, small variations were observed, primarily due to differences in loading conditions, particularly temperature fluctuations. These variations could potentially be minimized through the application of a temperature compensation technique, which will be explored in future studies. Overall, the results confirm a strong and repeatable linear relationship between ultrasonic velocity and rebar stress. This outcome demonstrates the feasibility of using a simple ultrasonic measurement setup for stress assessment in rebar, laying a solid foundation for future applications in nuclear concrete structure monitoring.

Table 6. Summary of the correlation slopes of tensile stress and ultrasonic velocity in all tests.

Test	Rebar size	Maximum stress (% yield stress)	Load rate (lb/s)	Cycles	Velocity–stress sensitivity k (loading)	Velocity–stress sensitivity k (unloading)
1	#8	34.4 ksi (57.3%)	25	1	-1.86×10^{-5}	-2.44×10^{-5}
2	#8	42.0 ksi (70.0%)	50	1	-2.67×10^{-5}	-2.55×10^{-5}
3	#8	53.5 ksi (89.1%)	50	4	$-(2.57\sim2.68) \times 10^{-5}$	$-(2.74\sim2.78) \times 10^{-5}$
4	#8	65.9 ksi (109.8%)	100	3	$-(2.75\sim2.77) \times 10^{-5}$	$-(2.74\sim2.77) \times 10^{-5}$
5	#6	40.8 ksi (68%)	50	2.5	$-(2.67\sim2.79) \times 10^{-5}$	$-(2.74\sim2.76) \times 10^{-5}$

Note: The load rate for Test 1 is reported as 25 lb/s in Table 6 for simplicity. The actual measured rate was 24.8 lb/s, as described in Section 5.1.

6. CONCLUSIONS

This study successfully demonstrated the feasibility of using ultrasonic NDE techniques based on the acoustoelastic effect for rebar stress measurement in lab. Through a series of well-controlled tensile tests on #8 and #6 Grade 60 steel rebar, the ultrasonic signals collected at different rebar stresses were processed by the use of advanced signal processing techniques, such as coda wave interferometry and the stretching algorithm, which enabled high-resolution detection of relative velocity changes. A consistent and repeatable linear relationship was observed between tensile stress and ultrasonic wave velocity. Tests were conducted across a range of loading conditions, varying in peak stress levels (up to 110% of yield) and loading rates (50–100 lb/s), to investigate the robustness and sensitivity of the acoustoelastic response.

The ultrasonic velocity exhibited a clear and measurable decrease during loading and increase during unloading, which is consistent with acoustoelastic theory. Across all tests (with the exception of the first), the calculated slopes of the velocity–stress correlation remained within a narrow range, between -2.65×10^{-5}/ksi and -2.79×10^{-5} based on the test results. Minor variations in these slopes were observed and are attributed primarily to temperature fluctuations and initial stress conditions, such as residual manufacturing stress. The thermoelastic effect, characterized by temperature decreases during elastic loading and increases during unloading, was consistently observed and further validated the physical basis of the ultrasonic response. Further efforts are needed to develop a temperature compensation technique to eliminate the temperature effect during the loading and unloading process or temperature fluctuations in a real ambient environment. Meanwhile, the experimental setup needs to be improved to avoid grip slip and sensor coupling failure.

Overall, the experimental results validate the linear acoustoelastic model for practical stress monitoring in steel rebar and support the implementation of ultrasonic NDE as a field-deployable diagnostic tool. This research lays a strong foundation for future development of non-invasive stress sensing systems in reinforced concrete structures, particularly in critical applications such as nuclear power plants and aging civil infrastructure.

Although the experiments in this study were conducted under controlled laboratory conditions, translating this setup to real-world field conditions will require further adaptation. Field deployment introduces challenges such as limited access to embedded rebar, variability in surface conditions, and environmental fluctuations. The current coupling method may not be practical in such settings, so future work should explore alternative coupling strategies (e.g., clamped or dry-point contact transducers) that are robust and repeatable under field conditions. Additionally, integrating automated temperature compensation and ruggedized sensor assemblies will be critical to ensure in-situ measurement reliability. Addressing these factors will be essential for extending the demonstrated laboratory methodology into a viable field-deployable monitoring system.

REFERENCES

[1] E. Tanala, G. Bourse, M. Fremiot, and J. F. De Belleval, "Determination of near surface residual stresses on welded joints using ultrasonic methods," *NDT & E International*, vol. 28, no. 2, pp. 83–88, Apr. 1995, doi: 10.1016/0963-8695(94)00013-A.

[2] M. Duquennoy, M. Ouaftouh, M. L. Qian, F. Jenot, and M. Ourak, "Ultrasonic characterization of residual stresses in steel rods using a laser line source and piezoelectric transducers," *NDT & E International*, vol. 34, no. 5, pp. 355–362, Jul. 2001, doi: 10.1016/S0963-8695(00)00075-X.

[3] A. Castellano, P. Foti, A. Fraddosio, S. Marzano, F. Paparella, and M. Daniele Piccioni, "Monitoring applied and residual stress in materials and structures by non-destructive acoustoelastic techniques," in *2016 IEEE Workshop on Environmental, Energy, and Structural Monitoring Systems (EESMS)*, Bari, Italy: IEEE, Jun. 2016, pp. 1–5. doi: 10.1109/EESMS.2016.7504830.

[4] C. Xu, W. Song, Q. Pan, H. Li, and S. Liu, "Nondestructive testing residual stress using ultrasonic critical refracted longitudinal wave," *Physics Procedia*, vol. 70, pp. 594–598, 2015, doi: 10.1016/j.phpro.2015.08.030.

[5] W. Song, C. Xu, Q. Pan, and J. Song, "Nondestructive testing and characterization of residual stress field using an ultrasonic method," *Chin. J. Mech. Eng.*, vol. 29, no. 2, pp. 365–371, Mar. 2016, doi: 10.3901/CJME.2015.1023.126.

[6] Y.-I. Hwang, G. Kim, Y.-I. Kim, J.-H. Park, M. Y. Choi, and K.-B. Kim, "Experimental measurement of residual stress distribution in rail specimens using ultrasonic LCR waves," *Applied Sciences*, vol. 11, no. 19, Art. no. 19, Jan. 2021, doi: 10.3390/app11199306.

[7] B. Zhong, J. Zhu, and G. Morcous, "Measuring acoustoelastic coefficients for stress evaluation in concrete," *Construction and Building Materials*, vol. 309, p. 125127, Nov. 2021, doi: 10.1016/j.conbuildmat.2021.125127.

[8] S. Zeng, C. Malone, and J. Zhu, "Temperature correction in acoustoelastic coefficient measurements," *NDT & E International*, vol. 140, p. 102959, Dec. 2023, doi: 10.1016/j.ndteint.2023.102959.

[9] Y.-W. Choi *et al.*, "Nondestructive evaluation of residual stress in shot peened inconel using ultrasonic minimum reflection measurement," *Materials*, vol. 16, no. 14, Art. no. 14, Jan. 2023, doi: 10.3390/ma16145075.

[10] L. F. He and S. Kobayashi, "Acoustoelastic determination of residual stress with laser doppler velocimetry," *Experimental Mechanics*, vol. 41, no. 2, pp. 190–194, Jun. 2001, doi: 10.1007/BF02323196.

[11] A. Karabutov *et al.*, "Laser ultrasonic diagnostics of residual stress," *Ultrasonics*, vol. 48, no. 6–7, pp. 631–635, Nov. 2008, doi: 10.1016/j.ultras.2008.07.006.

[12] R. M. Sanderson and Y. C. Shen, "Measurement of residual stress using laser-generated ultrasound," *International Journal of Pressure Vessels and Piping*, vol. 87, no. 12, pp. 762–765, Dec. 2010, doi: 10.1016/j.ijpvp.2010.10.001.

[13] M. Ya. Marusina, A. V. Fedorov, V. A. Bychenok, and I. V. Berkutov, "Ultrasonic laser diagnostics of residual stresses," *Meas Tech*, vol. 57, no. 10, pp. 1154–1159, Jan. 2015, doi: 10.1007/s11018-015-0595-4.

[14] Y. Zhan, C. Liu, X. Kong, and Z. Lin, "Experiment and numerical simulation for laser ultrasonic measurement of residual stress," *Ultrasonics*, vol. 73, pp. 271–276, Jan. 2017, doi: 10.1016/j.ultras.2016.08.013.

[15] Q. Pan, Y. Mi, Y. Wei, and Y. Ren, "A method of testing residual stress by ultrasonic shear and longitudinal waves," in *2016 IEEE International Conference on Mechatronics and Automation*, Aug. 2016, pp. 1295–1299. doi: 10.1109/ICMA.2016.7558749.

[16] F. Belahcene and J. Lu, "Determination of residual stress using critically refracted longitudinal waves and immersion mode," *The Journal of Strain Analysis for Engineering Design*, vol. 37, no. 1, pp. 13–20, Jan. 2002, doi: 10.1243/0309324021514790.

[17] W. Wang, C. Xu, Y. Zhang, Y. Zhou, S. Meng, and Y. Deng, “An improved ultrasonic method for plane stress measurement using critically refracted longitudinal waves,” *NDT & E International*, vol. 99, pp. 117–122, Oct. 2018, doi: 10.1016/j.ndteint.2018.07.006.
[18] N. Gandhi, J. E. Michaels, and S. J. Lee, “Acoustoelastic Lamb wave propagation in biaxially stressed plates,” *The Journal of the Acoustical Society of America*, vol. 132, no. 3, pp. 1284–1293, Sep. 2012, doi: 10.1121/1.4740491.
[19] R. Murayam and K. Misumi, “Development of a non-contact stress measurement system during tensile testing using the electromagnetic acoustic transducer for a Lamb wave,” *NDT & E International*, vol. 39, no. 4, pp. 299–303, Jun. 2006, doi: 10.1016/j.ndteint.2005.08.009.
[20] H. J. Lim and H. Sohn, “Online stress monitoring technique based on lamb-wave measurements and a convolutional neural network under static and dynamic loadings,” *Exp Mech*, vol. 60, no. 2, pp. 171–179, Feb. 2020, doi: 10.1007/s11340-019-00546-8.
[21] I. A. E. Agency, “Measurement of residual stress in materials using neutrons,” International Atomic Energy Agency, Text, 2005. Accessed: Mar. 17, 2025. [Online]. Available: https://www.iaea.org/publications/7215/measurement-of-residual-stress-in-materials-using-neutrons
[22] S. Harjo *et al.*, “Engineering & related studies at J-PARC,” *Materials Science Forum*, vol. 777, pp. 12–18, 2014, doi: 10.4028/www.scientific.net/MSF.777.12.
[23] H. Suzuki *et al.*, “Measuring strain and stress distributions along rebar embedded in concrete using time-of-flight neutron diffraction,” *Meas. Sci. Technol.*, vol. 25, no. 2, p. 025602, Jan. 2014, doi: 10.1088/0957-0233/25/2/025602.
[24] H. Suzuki *et al.*, “Application of neutron stress measurement to reinforced concrete structure,” in *Proceedings of the 2nd International Symposium on Science at J-PARC ? Unlocking the Mysteries of Life, Matter and the Universe ?*, vol. 8, in JPS Conference Proceedings, no. 8, vol. 8. , Journal of the Physical Society of Japan, 2015. doi: 10.7566/JPSCP.8.031006.
[25] H. Suzuki, K. Kusunoki, M. Kanematsu, T. Mukai, and S. Harjo, “Structural engineering studies on reinforced concrete structure using neutron diffraction,” presented at the Residual Stresses 10, Jan. 2017, pp. 25–30. doi: 10.21741/9781945291173-5.
[26] T. Koyama *et al.*, “Deformation analysis of reinforced concrete using neutron imaging technique,” presented at the Mechanical Stress Evaluation by Neutron and Synchrotron Radiation, May 2018, pp. 155–160. doi: 10.21741/9781945291678-24.
[27] A. Yasue *et al.*, “Accuracy of measuring rebar strain in concrete using a diffractometer for residual stress analysis,” *Quantum Beam Science*, vol. 7, no. 2, Art. no. 2, Jun. 2023, doi: 10.3390/qubs7020015.
[28] R. Yanagida, S. Fukada, and T. Sasaki, “Influence of rebar strength, pre-treatment, and measurement method on residual Stress measurement using portable X-ray diffractometer,” *Journal of Advanced Concrete Technology*, vol. 22, no. 7, pp. 391–405, 2024, doi: 10.3151/jact.22.391.
[29] K. Tong, J. Zhou, R. Zhao, W. Hu, Y. Qu, and C. Cheng, “Experimental study on rebar stress measurement based on force-magnetic coupling under excited magnetic field,” *Measurement*, vol. 189, p. 110620, Feb. 2022, doi: 10.1016/j.measurement.2021.110620.
[30] J. Xia, S. Zhang, L. Liao, H. Liu, and Y. Sun, “Working Stress Measurement of Prestressed Rebars Using the Magnetic Resonance Method,” *Buildings*, vol. 13, no. 6, Art. no. 6, Jun. 2023, doi: 10.3390/buildings13061416.
[31] J. Zhou, H. Ying, K. Tong, Y. Qu, H. Zhang, and R. Zhao, “Research on quantitative evaluation of rebar stress based on weak magnetic effect,” *Journal of Magnetism and Magnetic Materials*, vol. 573, p. 170635, May 2023, doi: 10.1016/j.jmmm.2023.170635.
[32] D. S. Hughes and J. L. Kelly, “Second-Order Elastic Deformation of Solids,” *Phys. Rev.*, vol. 92, no. 5, pp. 1145–1149, Dec. 1953, doi: 10.1103/PhysRev.92.1145.
[33] O. I. Lobkis and R. L. Weaver, “Coda-wave interferometry in finite solids: Recovery of P-to-S conversion rates in an elastodynamic billiard,” *Physical Review Letters*, vol. 90, no. 25, p. 254302, 2003.

[34] H. Sun, “Thermal Modulation of Nonlinear Ultrasonic Waves,” Ph.D., The University of Nebraska - Lincoln, United States -- Nebraska. Accessed: Jun. 01, 2023. [Online]. Available: https://www.proquest.com/docview/2444913300/abstract/D84F623EF6674299PQ/1
[35] M. A. Biot, “Thermoelasticity and irreversible thermodynamics,” *Journal of Applied Physics*, vol. 27, no. 3, pp. 240–253, Mar. 1956, doi: 10.1063/1.1722351.